



LAWRENCE  
LIVERMORE  
NATIONAL  
LABORATORY

# Universal Breakdown of Elasticity at the Onset of Material Failure

Craig Maloney, Anael Lemaitre

April 26, 2004

Physical Review Letters

## **Disclaimer**

---

This document was prepared as an account of work sponsored by an agency of the United States Government. Neither the United States Government nor the University of California nor any of their employees, makes any warranty, express or implied, or assumes any legal liability or responsibility for the accuracy, completeness, or usefulness of any information, apparatus, product, or process disclosed, or represents that its use would not infringe privately owned rights. Reference herein to any specific commercial product, process, or service by trade name, trademark, manufacturer, or otherwise, does not necessarily constitute or imply its endorsement, recommendation, or favoring by the United States Government or the University of California. The views and opinions of authors expressed herein do not necessarily state or reflect those of the United States Government or the University of California, and shall not be used for advertising or product endorsement purposes.

# Universal Breakdown of Elasticity at the Onset of Material Failure

Craig Maloney<sup>(1,2)</sup> and Anaël Lemaître<sup>(1,3)</sup>

<sup>(1)</sup> *Department of physics, University of California, Santa Barbara, California 93106, U.S.A.*

<sup>(2)</sup> *Lawrence Livermore National Lab - CMS/MSTD, Livermore, California 94550, U.S.A. and*

<sup>(3)</sup> *L.M.D.H. - Universite Paris VI, UMR 7603, 4 place Jussieu, 75005 Paris - France*

(Dated: April 19, 2004)

We show that, in the athermal quasi-static deformation of amorphous materials, the onset of failure is accompanied by universal scalings associated with a *divergence* of elastic constants. A normal mode analysis of non-affine (elastic) displacement fields, allows us to clarify their relation to the zero-frequency mode at the onset of failure and to crack-like patterns resulting from the full extent of a plastic event.

Experiments in nanoindentation of metallic glasses, [1] on granular materials [2] and on foams [3], show very intermittent stress fluctuations during a-thermal, quasi-static deformation of disordered materials. Related numerical studies include either MD simulations at very low strain rate, or “exact” implementation of a-thermal quasi-static deformation, which consists in alternating elementary steps of affine deformation with energy relaxation. [4] This protocol permits one to constrain the system to reside in a local minimum (inherent structure) at all times and observe the detailed mechanisms of elasto-plastic behavior in relation to the structure of the underlying potential energy landscape. As illustrated in figure 1, stress fluctuations arise from a series of reversible (elastic) branches correspond to deformation-induced changes of local minima. These branches are interrupted by sudden irreversible (plastic) events which occur when the inherent structure annihilates during a collision with a saddle point. [5]

Recent studies of both elasticity [6] and plasticity [5] have shown that striking properties arise solely from

the non-trivial structure of the potential energy landscape. Tanguy *et al* [6] have observed that, when the system follows *reversible* (elastic) changes of the inherent structures, molecules undergo large scale non-affine displacements. They observed that the existence of non-affine displacements is related to the breakdown of classical elasticity at small scales and quantitative differences between measured Lamé constants and their Born approximation. Malandro and Lacks [5] have shown that the destabilization of a minimum occurs through shear-induced collision with a saddle. At the collision, a single normal mode sees its eigenvalue going to zero. Building on this work, we studied the *irreversible* (plastic) event following the disappearance of an inherent structure: subsequent material deformation in search of a new minimum involves non-local displacement fields—in the likeness of nascent cracks—controlled by long-range elastic interactions. [7]

Several molecular displacement fields thus appear to be closely related to the geometrical structure of the potential energy landscape: (i) non-affine displacements along elastic branches, (ii) the single normal mode controlling the annihilation of an inherent structure, and (iii) the overall deformation occurring during an irreversible event. In order to piece together a complete picture of elasto-plasticity at the nanoscale, we need to understand the relation between these different fields and ask how elastic behavior breaks down at the onset of failure. It is thus a study of incipient plasticity—that is the onset of irreversible deformation—that we wish to perform.

We base our approach on microscopic expressions, and depart from previous studies of incipient failure [8] which are based on Hill’s continuum condition. [9] Indeed, a formal expression for the non-affine correction to elasticity is available, [10, 11] although it has entirely been overlooked by Tanguy *et al*. Here, we put such analytical tractions in perspective with the recent numerical developments, and use these expressions to construct a normal mode decomposition of the non-affine displacement field. This provides an analytical framework where it can be evidenced that the lowest frequency normal mode dominates the non-affine elastic displacement field close to a plastic transition. We then show that at any plastic

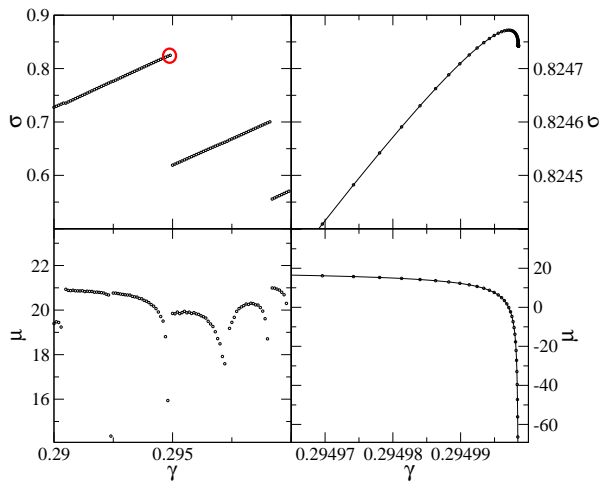


FIG. 1: Stress (top) and shear modulus (bottom) for a small strain interval about a strain of .3. Left: quasi-static deformation with fixed strain steps of size  $10^{-4}$ ; right: careful convergence to the circled yield point.

transition point, energy, stress, and the vibration frequencies display a singular, universal, behavior associated with a *divergence* of the elastic constants. The normal mode analysis of the subsequent cascade shows that the low frequency modes active at incipient plasticity are superseded by long-range elastic interactions in the latter stages of an irreversible event.

We consider in this work a molecular system in a periodic cell. The geometry of the cell is determined by the matrix  $h$  whose columns are the Bravais vectors. [12, 13] The affine deformation of the cell between configurations  $h_0$  and  $h$  is characterized by the Green-St Venant strain tensor,  $\underline{\underline{\epsilon}} = \frac{1}{2} \left( (h_0^{-1})^T \cdot h^T \cdot h \cdot h_0^{-1} - 1 \right)$ , which governs the elongation of a vector  $\overset{\circ}{\vec{x}} \rightarrow \vec{x}$ , as  $\vec{x}^2 = \overset{\circ}{\vec{x}}^2 + 2 \overset{\circ}{\vec{x}}^T \cdot \underline{\underline{\epsilon}} \cdot \overset{\circ}{\vec{x}}$ . As the energy functional generally depends only on the set of interparticle distances, it can be parametrized as  $\mathcal{U}(\{\overset{\circ}{\vec{r}}_i\}, \underline{\underline{\epsilon}})$  where  $\{\overset{\circ}{\vec{r}}_i\}$  are the positions of the particles in a *reference* cell. [10, 14] Varying,  $\underline{\underline{\epsilon}}$  for fixed  $\{\overset{\circ}{\vec{r}}_i\}$  corresponds to an affine displacement of the molecules in real space.

To start, let's contemplate more closely the athermal, quasi-static algorithm. Deformation,  $\underline{\underline{\epsilon}}(\gamma)$ , is enforced by moving the Bravais axes of the periodic cell;  $\gamma$  is introduced as rescaled coordinate which measures the amount of deformation from some reference state. In practice  $\underline{\underline{\epsilon}}(\gamma)$  corresponds to either pure shear or pure compression. Formally, the limit  $h_0 = h$  (or  $\gamma \rightarrow 0$ ) is often appropriate to define stresses and elastic constant around a (possibly stressed) reference state. Once a choice of  $h_0$  is made, the algorithm tracks in the reference cell a trajectory  $\{\overset{\circ}{\vec{r}}_i(\gamma)\}$ , which is implicitly defined by demanding that the system remain in mechanical equilibrium: [10, 11]

$$\forall i \quad , \quad \vec{F}_i \equiv \left. \frac{\partial \mathcal{U}}{\partial \overset{\circ}{\vec{r}}_i} \right|_{\{\overset{\circ}{\vec{r}}_j\}, \gamma} = \vec{0} \quad . \quad (1)$$

Starting at mechanical equilibrium at  $\gamma = 0$ ,  $\{\overset{\circ}{\vec{r}}_i(\gamma)\}$  is a continuous function of  $\gamma$  on some interval  $[0, \gamma_c]$ . At  $\gamma_c$ , the local minimum collides with a saddle point. [5]

An equation of motion for  $\vec{\mathbf{r}} = \{\overset{\circ}{\vec{r}}_i(\gamma)\}$  is obtained by derivation of (1) with respect to  $\gamma$ . Denoting,  $\mathcal{H} = \left( \frac{\partial^2 \mathcal{U}}{\partial \overset{\circ}{\vec{r}}_i \partial \overset{\circ}{\vec{r}}_j} \right)$ ,  $\underline{\underline{\Xi}} = \left( \frac{\partial^2 \mathcal{U}}{\partial \overset{\circ}{\vec{r}}_i \partial \gamma} \right)$ , and  $\underline{\underline{\Xi}}_{\alpha\beta} = \left( \frac{\partial^2 \mathcal{U}}{\partial \overset{\circ}{\vec{r}}_i \partial \epsilon_{\alpha\beta}} \right)$ , we find:

$$\frac{d\vec{\mathbf{r}}}{d\gamma} = -\mathcal{H}^{-1} \cdot \underline{\underline{\Xi}} = -\mathcal{H}^{-1} \cdot \sum_{\alpha\beta} \underline{\underline{\Xi}}_{\alpha\beta} \frac{d\epsilon_{\alpha\beta}}{d\gamma} \quad . \quad (2)$$

This relation holds for any  $\gamma \in [0, \gamma_c]$ . The inverse of  $\mathcal{H}$  is defined up to translation modes: this can be done either by fixing the position of a molecule, or by reindexing all the sums on the pairs, instead of the molecules. In the limit  $h \rightarrow h_0$ ,  $\mathcal{H}$  is thus the Dynamical Matrix.  $d\vec{\mathbf{r}}/d\gamma$  is a rescaled “velocity” of molecules in quasi-static deformation. It defines the direction (in tangent space) of the non-affine displacement field observed by Tanguy

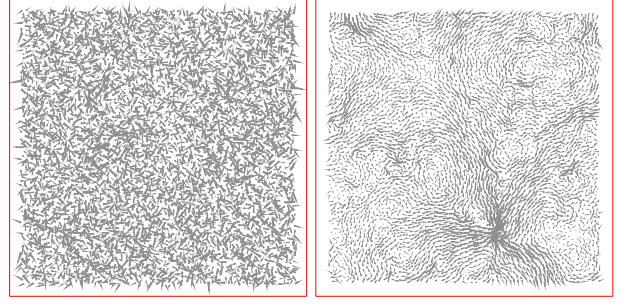


FIG. 2: a) The force response to simple shear,  $\underline{\underline{\Xi}}$ , at a strain configuration,  $\gamma = 0.2945$ , or  $\gamma_c - \gamma \sim 10^{-4}$ . b) The non-affine velocity (or “displacement”) field,  $\frac{d\vec{\mathbf{r}}}{d\gamma}$  for the same state as in a).

*et al* and can be directly evaluated by solving equation (2) without resorting to quadruple precision minimization. [6]

Here, we illustrate these idea from numerical simulations of a two-dimensional polydisperse mixture of particles interacting through a shifted Lennard-Jones potential. [6] Particle sizes  $r_S = r_L \sin \frac{\pi}{10} / \sin \frac{\pi}{5}$  and a number ratio  $N_L/N_S = \frac{1+\sqrt{5}}{4}$  are used to prevent crystallization. We have also performed simulations on Hertzian spheres which yield results consistent with those of the Lennard-Jones system discussed below. Typical patterns of the fields  $\underline{\underline{\Xi}}$  and  $d\vec{\mathbf{r}}/d\gamma$  in (steady) simple shear deformation are shown figure 2: the apparent small scale randomness of the vector  $\underline{\underline{\Xi}}$  is in sharp contrast with the large vortex-like structures displayed by the non-affine “velocity” field  $d\vec{\mathbf{r}}/d\gamma$ . To understand the randomness of  $\underline{\underline{\Xi}}$ , note that  $\underline{\underline{\Xi}}_i = \partial \vec{F}_i / \partial \gamma$  is the force response on molecule  $i$  after an elementary affine deformation of the system: it only depends on the configuration of the molecules with which molecule  $i$  interacts, hence is an  $\underline{\underline{\epsilon}}$ -dependent measure of the local disorder of molecular configurations. We checked that spatial correlation decay very fast in field  $\underline{\underline{\Xi}}$ : in the following discussion, the short-range randomness of the field  $\underline{\underline{\Xi}}$  allows us to interpret it as noise.

An analytical expression for the bulk elastic constants derives along similar lines. [10, 11] The first derivative of the potential with respect to the components of  $\underline{\underline{\epsilon}}$  defines the thermodynamic stress,  $\underline{\underline{t}}$ :  $t_{\alpha\beta} = \frac{1}{V_0} \frac{d\mathcal{U}}{d\epsilon_{\alpha\beta}} = \frac{1}{V_0} \frac{\partial \mathcal{U}}{\partial \epsilon_{\alpha\beta}}$ . The total derivative indicates derivation while preserving mechanical equilibrium, the second equality results from equation (1), and  $V_0$  is the volume of the simulation cell. The second (total) derivative of the energy gives the elastic constants, [14]

$$C_{\alpha\beta\chi\sigma} = \frac{1}{V_0} \left( \frac{\partial^2 \mathcal{U}}{\partial \epsilon_{\alpha\beta} \partial \epsilon_{\chi\sigma}} + \sum_j \frac{\partial^2 \mathcal{U}}{\partial \overset{\circ}{\vec{r}}_i \partial \epsilon_{\alpha\beta}} \cdot \frac{d\overset{\circ}{\vec{r}}_i}{d\epsilon_{\chi\sigma}} \right) \quad . \quad (3)$$

We recognize the first term as being the Born approximation  $C_{\alpha\beta\chi\sigma}^{\text{Born}}$ . The second term accounts for the non-affine

corrections, and reads:  $\tilde{C}_{\alpha\beta\chi\sigma} = -\frac{1}{V_0}\tilde{\Xi}_{\alpha\beta}\cdot\mathcal{H}^{-1}\cdot\tilde{\Xi}_{\chi\sigma}$ . Similarly, the second derivatives of the energy, following any generic deformation  $\underline{\Xi}(\gamma)$ , can be written as:

$$\frac{d^2U}{d\gamma^2} = \frac{\partial^2U}{\partial\gamma^2} - \tilde{\Xi}\cdot\mathcal{H}^{-1}\cdot\tilde{\Xi} \quad (4)$$

For an isotropic material, the elastic constants can be written:  $C_{\alpha\beta\chi\sigma} = \lambda\delta_{\alpha\beta}\delta_{\chi\sigma} + \mu(\delta_{\alpha\chi}\delta_{\beta\sigma} + \delta_{\alpha\sigma}\delta_{\beta\chi})$ , which define the Lamé constants,  $\lambda$  and  $\mu$ . In order to estimate these constants, it is not necessary to evaluate all the components of the tensor  $\tilde{\Xi} = (\tilde{\Xi}_{\alpha\beta})$ , but only two of its projections  $\tilde{\Xi}$ , *e.g.* for pure shear and pure compression and use equation (4). In equation (4) the correction to the Born term is negative definite: quantities such as the shear modulus,  $\mu$ , or the compressibility,  $K = \lambda + \mu$ , are necessarily smaller than the Born term, while this is not necessarily true of  $\lambda = K - \mu$  alone as it does not, by itself, correspond to any realizable mode of deformation. This is consistent with the numerical observations by Tanguy *et al* [6] in Lennard-Jones systems.

Next, we perform a normal mode analysis of the fields  $\tilde{\Xi}$ . Denoting  $\tilde{\Psi}_p$  the eigenvectors of the Dynamical Matrix (normal modes), and  $\lambda_p = (\omega_p)^2$  the associated eigenvalues, the vector  $\tilde{\Xi}$  can be decomposed as:  $\tilde{\Xi} = \sum_p \xi_p \tilde{\Psi}_p$ , with  $\xi_p = \tilde{\Xi}\cdot\tilde{\Psi}_p$ . If  $\tilde{\Xi}$  is a random field, the variables  $\xi_p$  are random. From this decomposition, expressions can be obtained for the non-affine direction and for the non-affine contribution to elasticity:

$$\frac{d\tilde{\mathbf{r}}}{d\gamma} = -\sum_p \frac{\xi_p}{\lambda_p} \tilde{\Psi}_p \quad \text{and} \quad C_{\underline{\Xi}} = -\sum_p \frac{\xi_p^2}{\lambda_p} \quad (5)$$

We now concentrate on the behavior of the shear modulus at incipient plasticity, as shown in figure 1 and 3. Malandro and Lacks have shown numerically that at the onset of a plastic event a single eigenfrequency goes to zero. [5] We denote  $\tilde{\Psi}^*(\gamma)$  the first non-zero normal mode; in two dimensions, it is the third in the spectrum. Close to failure ( $\gamma \rightarrow \gamma_c$ ),  $\lambda^*(\gamma) \rightarrow 0$ , hence  $\tilde{\Psi}^*(\gamma_c)$  must dominate the non-affine direction  $d\tilde{\mathbf{r}}/d\gamma$ . This is true if and only if the quantity  $\xi^*(\gamma) = \tilde{\Psi}^*(\gamma)\cdot\tilde{\Xi}(\gamma)$  does not vanish at the yield point.

In order to check this scenario, we have performed numerical simulations of the same 2D binary mixture described above. We note that, on approaching a plastic event, caution must be taken to correctly minimize the energy without using a quadratic approximation. We observe that (i) the mode  $\tilde{\Psi}^*$  is localized close to failure while (ii)  $\tilde{\Xi}(\gamma) \rightarrow \tilde{\Xi}(\gamma_c)$  remains noisy and weakly correlated with the normal modes. As a consequence of this observation,  $\xi^*(\gamma)$  has a random, but typically non-zero limit when  $\gamma \rightarrow \gamma_c$ . The non-affine field is dominated by  $-\xi^*(\gamma_c)/\lambda^*(\gamma) \times \tilde{\Psi}^*(\gamma_c)$  and the non-affine correction to elasticity by  $\tilde{\mu} \sim -(\xi^*)^2/\lambda^*$  which diverges toward  $-\infty$ . In contrast, the Born term—which depends on the

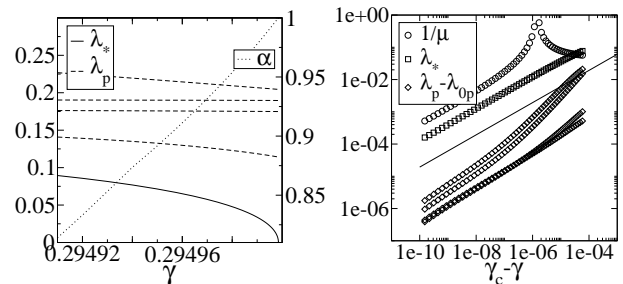


FIG. 3: a) relative participation of the lowest normal mode in the non-affine elastic displacement field,  $\alpha^* \doteq (\xi^*/\lambda^*)^2 / \sum_p (\xi_p/\lambda_p)^2$  (solid black); lowest eigenvalue of the dynamical matrix (dotted red); next several eigenvalues (dashed green). b) In log-log scale (as a guide to the eye, the thick black line is  $\sqrt{\gamma_c - \gamma}$ ):  $1/\mu$  (black circles); lowest eigenvalue (red squares); next several eigenvalues minus their terminal values (green diamonds).

pair-correlation only— does not present any divergence. Since the Lamé constant  $\mu = \mu^{\text{Born}} + \tilde{\mu}$ , on approaching failure, the system reaches a point  $\gamma_0 < \gamma_c$  at which  $\tilde{\mu} = -\mu^{\text{Born}}$ , whence  $\mu$  vanishes. For  $\gamma \in [\gamma_0, \gamma_c]$ , the material is unstable to any constant applied stress: this region is accessible to us because deformation—and not stress—is prescribed.

In order to understand more specifically how the elastic constants behave close to  $\gamma_c$ , let us consider the functions  $\lambda_p(\gamma)$ , which are continuous on a small interval close to  $\gamma_c$  (the second derivatives of the potential are supposed to be regular). Close to the yield point,  $\gamma_c$ , the deformation is dominated by the lowest normal mode:  $\tilde{\mathbf{r}}(\gamma) - \tilde{\mathbf{r}}(\gamma_c) \sim x(\gamma)\tilde{\Psi}^*(\gamma_c)$ . (We project the deformation on the mode  $\tilde{\Psi}^*$  at the yield point.) From this relation and (5), we obtain the dominant contribution:  $dx/d\gamma \sim -\xi^*(\gamma_c)/\lambda^*(\gamma)$ . The coordinate  $x$  measures a true displacement in configuration space: we expect that no singular behavior occurs in this rescaled coordinate whence,  $\lambda^*(x)$  should vanish regularly,  $\lambda^*(x) \sim ax$  close to  $x = 0$ . From this assumption, it results:  $x(\gamma) \sim \sqrt{2\xi^*(\gamma_c)(\gamma_c - \gamma)/a}$ . This relation controls entirely the behavior of all observables when approaching the yield point: any observable  $A$  which behaves regularly as a function of  $x$  (any regular function of molecular configurations) “accelerates” close to the yield point:  $dA/d\gamma \sim 1/\sqrt{\gamma_c - \gamma}$ . In particular, we obtain,  $d\tilde{\mathbf{r}}/d\gamma \sim \tilde{\Psi}_p/\sqrt{\gamma_c - \gamma}$ , and  $\lambda^*(\gamma) = \sqrt{2a\xi^*(\gamma_c - \gamma)}$ , whence,  $\tilde{\mu} \sim -(\xi^*)^3/2/\sqrt{2a(\gamma_c - \gamma)}$ . We could observe these scalings numerically by a careful approach to the yield point, as shown figure 3. A similar divergence is observed for the compression modulus, but with a different prefactor, determined by the normal mode decomposition of the  $\tilde{\Xi}$  field associated to pure compression.

We now turn to the overall plastic event following failure (see figure 4 and 5). We have already shown, in similar atomistic systems, that any single plastic event

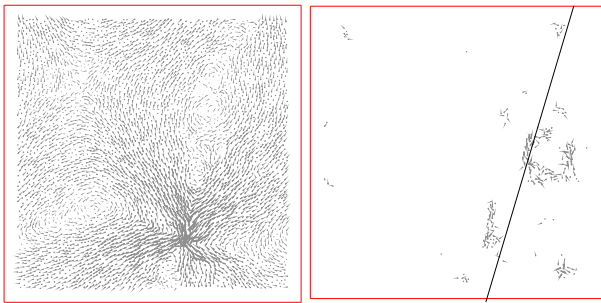


FIG. 4: a) Non-affine elastic displacement field at a distance  $\gamma_c - \gamma \sim 10^{-10}$  from the transition. Note the quadrupolar alignment with the direction of applied strain. b) The local relative displacement field (the displacement of each particle measured with respect to the average displacement of its neighbors) which is incurred after the entire plastic cascade. The solid line is a guide to the eye oriented along the oblique Bravais axis.

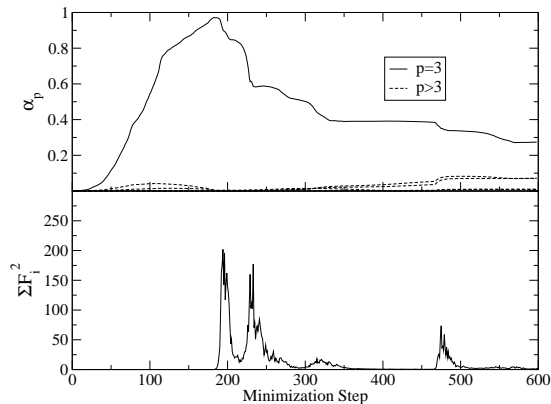


FIG. 5: Evolution of the displacement field during the irreversible cascade corresponding to the event circled in figure 1. Top: contribution  $\alpha^*$  (solid line) of the critical mode and  $\alpha_p(t)$  (dashed line) of the next five modes to the displacement field. Bottom: sum of the squares of the forces on the particles.

involves a cascade of local rearrangements. [7] Our preceding work suggested that the overall plastic event was controlled by long range elastic interactions and differed from the displacement fields which dominate the onset of failure. Our present normal mode decomposition allows us to gain more insight on this process. Writing  $\vec{r}(t) - \vec{r}(0) = \sum_p \Delta \xi_p(t) \vec{\Psi}_p(\gamma_c)$ , we extract the quantities  $\alpha_p \doteq (\Delta \xi_p(t))^2 / \sum_p (\Delta \xi_p(t))^2$ , which are shown figure 5 for the lowest frequency modes. To trigger the relaxation, we shear the system forward by a small amount of shear,  $\gamma - \gamma_c \sim 10^{-5}$ . The initial affine displacement serves as a perturbation and projects randomly on the normal modes, whence the contributions  $\alpha_p$  start around zero. We observe that (i) the initiation of the cascade is clearly

dominated by the critical mode (ii) this effect suddenly stops before reaching the first peak in  $\sum_i F_i^2$  (this peak correspond to the first inflection point of energy vs.  $t$  during the descent) (iii) the subsequent displacement appears to be random, when projected on the lowest part of the spectrum, indicating that low frequency normal modes are irrelevant for the latter stages of plastic failure. The system escapes its initial inherent structure in the direction of the lowest normal mode, whereas, in the late stages of a plastic event the emergence of long-range elastic interactions supersedes the low energy modes responsible for the onset of failure.

To conclude, we wish to stress that we expect our analysis to apply to many materials, to modes of deformation other than uniform shear, and to several experimental protocols at the nanoscale, including nanoindentation studies or material deformation induced by an AFM tip. Knowing the detailed behavior of elastic constants at incipient plasticity opens the route toward a possible control of material deformation at the nanometer scale.

This work was partially supported under the auspices of the U.S. Department of Energy by the University of California, Lawrence Livermore National Laboratory under Contract No. W-7405-Eng-48, by the NSF under grants DMR00-80034 and DMR-9813752, by the W. M. Keck Foundation, and EPRI/DoD through the Program on Interactive Complex Networks. CM would like to acknowledge the guidance and support of V. V. Bulatov and J. S. Langer and the hospitality of LLNL University Relations.

- 
- [1] C. A. Schuh and T. G. Nieh, *Acta Mater.* **51**, 87 (2003).
  - [2] B. Miller, C. O'Hern, and R. P. Behringer, *Phys. Rev. Lett.* **77**, 3110 (1996).
  - [3] E. Pratt and M. Demin, *Phys. Rev. E* **67**, (2003).
  - [4] K. Maeda and S. Takeuchi, *J Phys-F-Metal Phys* **8**, L283 (1978).
  - [5] D. L. Malandro and D. J. Lacks, *J. Chem. Phys.* **110**, 4593 (1999).
  - [6] A. Tanguy, J. P. Wittmer, F. Leonforte, and J.-L. Barrat, *Phys. Rev. B* **66**, 174205 (2002).
  - [7] C. Maloney and A. Lemaitre, *cond-mat/0402148*.
  - [8] J. Li *et al.*, *Nature* **418**, 307 (2003).
  - [9] R. Hill, *J. Mech. Phys. Sol.* **10**, 1 (1962).
  - [10] D. Wallace, *Thermodynamics of Crystals* (Wiley, New York, 1972).
  - [11] J. F. Lutsko, *J. Appl. Phys.* **64**, 1152 (1988).
  - [12] J. Ray and A. Rahman, *J. Chem. Phys.* **80**, 4423 (1984).
  - [13] J. Ray and A. Rahman, *Phys. Rev. B* **32**, 733 (1985).
  - [14] T. Barron and M. Klein, *proc. Phys. Soc.* **85**, 523 (1965).